Iranian Journal of Geophysics, Vol 16 No 4, 2023, Page 165 – 174 (Research Article)
DOI: 10.30499/IJG.2022.363439.1458

Fault-kinematic and stress state investigation using focal mechanism solution along the Mosha fault, Alborz Mountain: implication for changing stress tectonic regime

Mohsen Azghandi[1], Mohammad Reza Abbassi[2*], Gholam Javan-Doloei[2] and Ahmad Sadidkhouy[3]

[1]*Ph.D. Candidate in Seismology, International Institute of Earthquake Engineering and Seismology, Tehran, Iran*
[2]*Associate Professors, Seismological Research Center, International Institute of Earthquake Engineering and Seismology, Tehran, Iran*
[3]*Assistant Professor, Institute of Geophysics, University of Tehran, Tehran, Iran*

(Received: 24 September 2022, Accepted: 26 October 2022)

Abstract

Investigation of historical and instrumental seismicity and fault kinematics of major faults are used to deduce the stress state in the northeast of Greater Tehran. In the present study, we have identified the Mw 5.1 earthquake and its related aftershocks in northeast Tehran that occurred on May 7, 2020. In this regard, after combining the waveforms of seismograms recorded in the seismic stations of Tehran and neighbouring provinces, the location, magnitude, and exact time of occurrence of the main shock and its six aftershocks have been calculated. Then, using three methods, including waveform modelling, P wave polarity and the ratio of P and S wave amplitudes, the focal mechanism of the fault causing seismic events is estimated. Fault kinematic study and the epicenter of the seismic event and related aftershocks suggest that the Mosha fault could be responsible for the event. Furthermore, the regional tectonic stress field has been calculated by focal mechanism inversion. Comparisons between stress field orientations and stress ratio provide new information on the local stress field. The variation of the stress ratio in the lower and upper crust is considerably high, demonstrating an inhomogeneity of deformation related to the Mosha fault.

Keywords: Waveform modelling, Mosha fault, 3D stress tensor, northeastern Tehran earthquake

*Corresponding author: abbassi@iiees.ac.ir

1 Introduction

The tectonic activity in the Alborz Mountain, northern Iran, is due to the northward convergence of Central Iran toward Eurasia and the northwestward motion of the southern Caspian basin concerning Eurasia. Previously proposed models suggested that the NW component of the movement resulting from the clockwise rotation of the South Caspian block is responsible for left lateral motion on the NW trending faults in the western Alborz. Recent GPS studies indicate that northern Iran, including north Central Iran, Alborz Mountains, and the South Caspian block, are rotating clockwise concerning Eurasia (e.g., koyi et al., 2016). This rotation is responsible for the formation of several E-W striking extensional basins. Two prominent faults along the southern Central Alborz are the Mosha and the North Tehran fault. The Mosh fault, located immediately in the eastern branch of central Alborz, has experienced some historical earthquakes along its different segments (Tchalenko 1974; Ambraseys & Melville 1982; Berberian 1983; Berberian & Yeats 2001). The Mosh fault, with a more than 175 km length, strikes E–W to WNW–ESE, and dips between 35◦ and 70◦ (Tchalenko 1974; Allen *et al.* 2003).

Previous seismic studies regarding the faulting mechanisms of the Mosha fault are controversial (e.g. Tatar et al., 2012; Momeni and Madariaga, 2022). Some geological data, such as fault kinematics, suggest strike-slip with reverse components (Bachmanov et al., 2004). According to previously published geodynamic concepts, the Alborz region was subjected to a series of extensional and compressional tectonic processes, ultimately linked with the opening and closure of the Tethys Ocean and related basins and clockwise rotations of the basement (e.g. Ballato et al., 2011; Hessami.,2020). A recent study has shown an extensional component accompanying strike-slip faulting (Abbassi, 2020). Notably, the establishment of present-day stress seems relatively young (Abbassi and Shabanian, 1999). Therefore, a seismic study together with a field investigation on the hanging wall of the Mosha has been conducted to understand the true nature of the fault and its seismic threat to Greater Tehran.

Recently, an earthquake occurred in the crust of northeast Tehran on May 5, 2020, with a magnitude of 5.1. In addition, sixteen aftershocks larger than 2.5 occurred during two years around the aforementioned main shock. So, the main goal of this paper is to find a reliable focal mechanism solution for this earthquake to answer the question of the faulting mechanism of the Mosha fault. Geological observations, seismic studies, and stress state in this region can be constructive for assessing earthquake hazards, and the resilience of buildings and lifeline infrastructures for Tehran city. Reactivating the Mosha fault near the eastern part of Tehran's metropolitan area may severely damage the densely populated capital of Iran.

2 Methodology and Data

We used The waveform data set in this study provided by the Iranian Seismological Center (IRSC) and the Iranian National Broadband Seismic Network (INSN) for the focal mechanisms solution. The information on seismic stations is presented in table 2. We also implemented earthquake fault plane solutions from other studies (Tatar et al., 2012; Nemati et al., 2011; Yaminifar et al., 2018; Soltanimoghadam et al., 2018) to examine stress field.

Three methods, including waveform modelling using ISOLA code, P wave polarity, and the ratio of P and S wave amplitude, are implemented to estimate the focal mechanisms of the mainshock and its aftershocks. In the next step, we examine the stress field in Central Alborz using a refined stress inversion methodology of focal mechanisms data. The whole study

area is subdivided into Voronoi cells by K_Means based on seismic depth and horizontal variation. We apply the refined stress inversion method of Martínez-Garzón, Ben-Zion, et al. (2016) developed on the double-couple earthquake focal mechanism catalogue in central Alborz. The inversion method employs the refined MSATSI software (Martínez-Garzón et al., 2014; Martínez-Garzón, Ben-Zion, et al., 2016), which is an updated version of the SATSI algorithm (Hardebeck & Michael, 2006; Michael, 1984). The stress inversion includes the following assumptions: (1) The stress field is homogeneous within a considered rock volume, (2) earthquakes occur on preexisting faults with varying orientations, and (3) slip on each fault occurs parallel to the direction of its tangential traction (Bott, 1959; Wallace, 1951). The linear damped stress inversion is applied to reduce potential data discretization artifacts (Hardebeck & Michael, 2006). The performed inversion estimates the orientations of the three principal stresses σ1, σ2, and σ3 (from most to least compressive) and the stress ratio parameter, R, defined as $R = \frac{\sigma_1 - \sigma_2}{\sigma_1 - \sigma_3}$ (The stress ratio (R-value) ranges between 0 and 1, with smaller and larger stress ratios in a strike-slip environment corresponding to stress regimes closer to transtensional (i.e., mixed strike-slip and normal faulting) and transpressional (i.e., mixed strike-slip and reverse faulting) fields, respectively. The orientation of maximum horizontal compressional stress, SHmax, is computed from the orientation of the principal stress axes following Lund and Townend (2007), and the estimated trends and plunges of the principal stresses are classified into Andersonian stress regimes: normal, strike-slip, and reverse, and oblique faulting types (Zoback, 1992). Uncertainty estimations of the inversion outputs are obtained by bootstrap resampling the original focal mechanisms (Michael, 1987) and providing 95% confidence intervals.

3 Results and Observations

We determined seven focal mechanisms, including the main earthquake and six aftershocks. Details of all focal mechanisms are given in table 1. Two are solved with waveform modelling using ISOLA code, and others by the polarity of the P wave and the ratio of P and S wave amplitude.

Most of the focal mechanisms show a strike-slip faulting mechanism with a reverse component. Only one of them displays a normal component. This changing of the mechanism types can be related to inhomogeneity of the stress regime. The field visit at four stations was carried out on the hanging wall of the Mosha fault to deduce the faulting mechanism based on our observation measurements.

Outcrops of the Mosha fault (as shown in Fig.1) at station 1 show limestone rocks separating alluvial sediments. The alluvial deposit covers both sides of the rock formation. The fault dips about 20-45 degrees facing the North and South. The Dashed lines denote the dip variations of alluvial deposits. The fault kinematic measurements are drawn on the stereo plots. These results show the mechanisms of the Mosha fault include both extensional and compressional components. The circles in the stereo-plots show the P axis of measurements on rocks. The dispersion of stress axes and different mechanisms indicate that this fault underwent various tectonic stresses. The grain size heterogeneity suggests a glacial deposit covering the rock mass in an outcrop 1, (Fig. 2). The distance between outcrops 1 and 3 is 500 meters. Across this distance, rock formation and alluvium have been deformed under several tectonic events.

Furthermore, this distance defines the hanging wall of the Mosha fault zone. In the area of outcrop 2 (Fig.1), we observe some E-W faulting with dominant dip-slip (extensional) movement and occasionally dextral components. The location of outcrop 3 marks the last station that has been influenced by the fault movements

(Fig.3). The young tectonic activity is responsible for the folded young alluvial deposit (it is thought to be the Late Pleistocene in age). The northern edge of this fold dips toward the North about 15 degrees. The folded layers are shown with white dashed lines in Fig. 3. It is noted that the strike-slip faulting is accompanied by an extensional component (Fig. 3). The close-up view of this section illustrated in figure 3b shows the tilting of the alluvial layers towards the South with a dashed line. The mechanism of faults in the southern ridge is in agreement with the modern stress state in central Alborz. The circle in the stereo plots shows the maximum horizontal stress axis. As shown, this outcrop defines two tectonic events. In the first step, the contractional deformation led to folding. Later, strike-slip faults with an extensional component influenced the southern limb of young folded strata (Fig. 3c).

Table 1. The parameters of focal mechanisms solution of the main earthquake on May 7 2020, its aftershocks using waveform modelling (highlighted with yellow) and P wave polarity, and the ratio of P and S wave amplitude.

Date	Hour	Lat. (°)	Long. (°)	Strike (°)	dip(°)	rake(°)	Method
20200507	20:18	35.78	52.05	289	61	10	Waveform modeling
20200507	21:49	35.79	52.02	147	60	84	Polarity &Amplitude Ratio
20200507	22:22	35.81	51.98	288	56	10	Polarity &Amplitude Ratio
20200509	12:11	35.80	51.96	287	82	16	Polarity &Amplitude Ratio
20200509	22:18	35.79	52.05	302	85	-19	Polarity &Amplitude Ratio
20200509	22:21	35.79	51.99	302	55	55	Polarity &Amplitude Ratio
20200527	09:11	35.79	52.04	303	44	44	Waveform modeling

Table 2. The list of the stations used for focal mechanisms solution.

Station	Lat. (°)	Long. (°)
CHTH	35.908	51.126
DAMV	35.63	51.971
GHVR	34.48	51.295
GLO	36.5024	53.8309
HSB	35.4275	51.3567
KHMZ	33.739	49.959
KRBR	29.982	56.761
NASN	32.799	52.808
QABG	35.70846	49.58238
SFB	34.3519	52.2407
SNGE	35.093	47.347
THE	35.7519	51.3892
THKV	35.916	50.879
VRN	34.9953	51.7272
YZKH	32.455	54.677
ZNJK	36.67	48.685

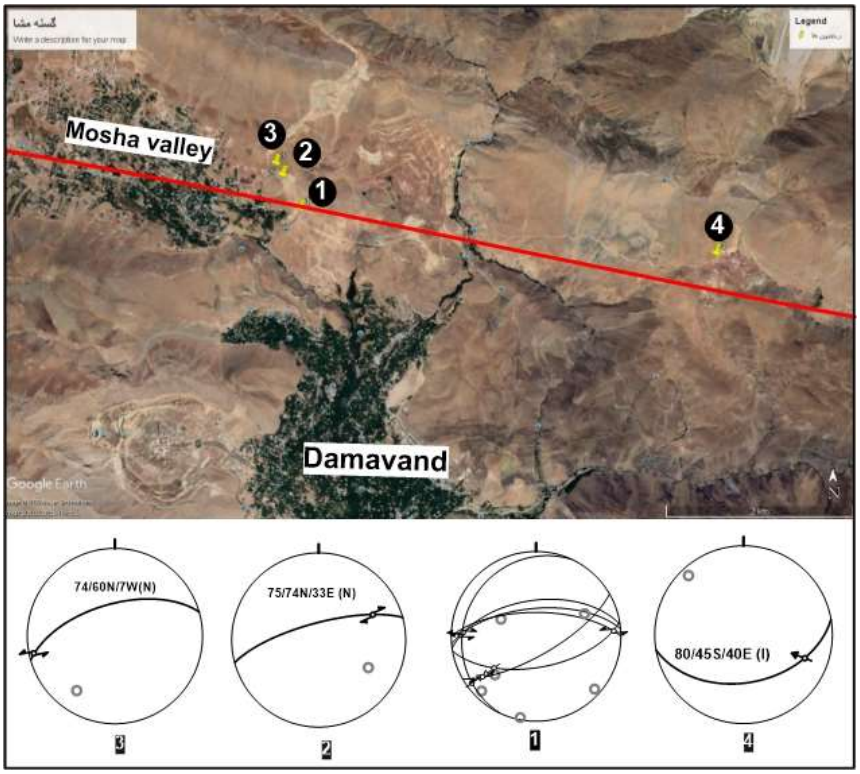

Figure 1. Overview map in google earth of the Mosha fault extended from northeast Damavand to Mosha valley. The numbers on the map demonstrate the locations of the visit measurements. Four stereo plots are related to fault kinematic measurements in satisfied stations. The circles in the stereo plots show the P axis.

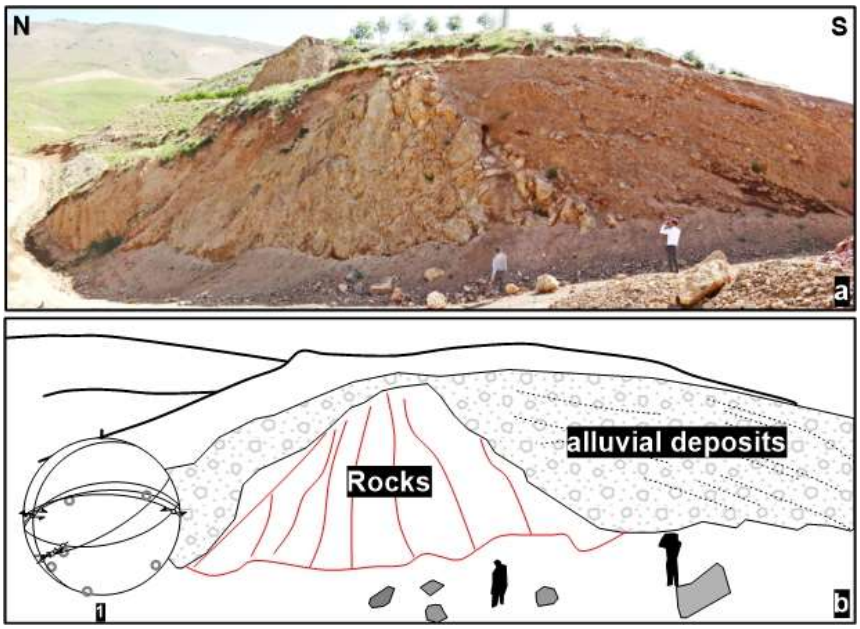

Figure 2. The outcrops of the Mosha fault near the Mosha valley in station 1 are indicated in Fig. 1. The limestone rocks are placed between two alluvial sediment layers. The dip variations of alluvial deposits are demonstrated with dashed lines.

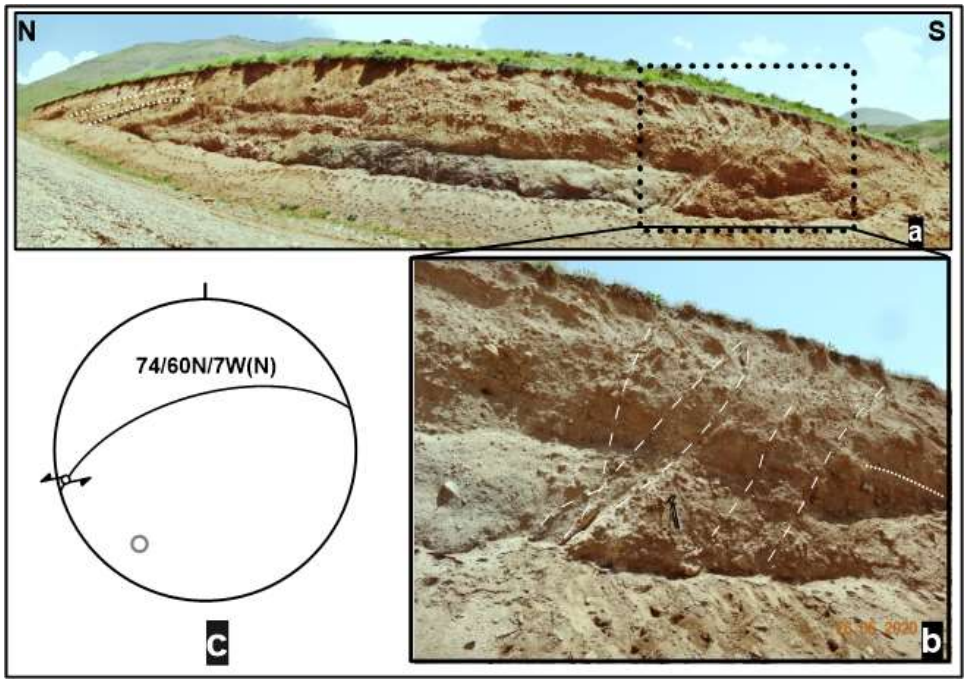

Figure 3. a) The folded of glacial formations at outcrop 3 affected the southern edge of it by transtensional fault. b) The close-up view of this faulting, c) The circle in the stereo-plot shows the maximum horizontal stress axis.

The measurements in Outcrop 4 (Fig.4) show compressive faulting with a horizontal dextral component which affected the inhomogeneous alluvial deposit. The inhomogeneity in grain size suggests a glacial deposition. The stereographic image of this fault at the bottom of figure 4. on the right side shows oblique reverse faulting with a right lateral component, which is consistent with a NW-directed horizontal maximum stress direction (SHmax).

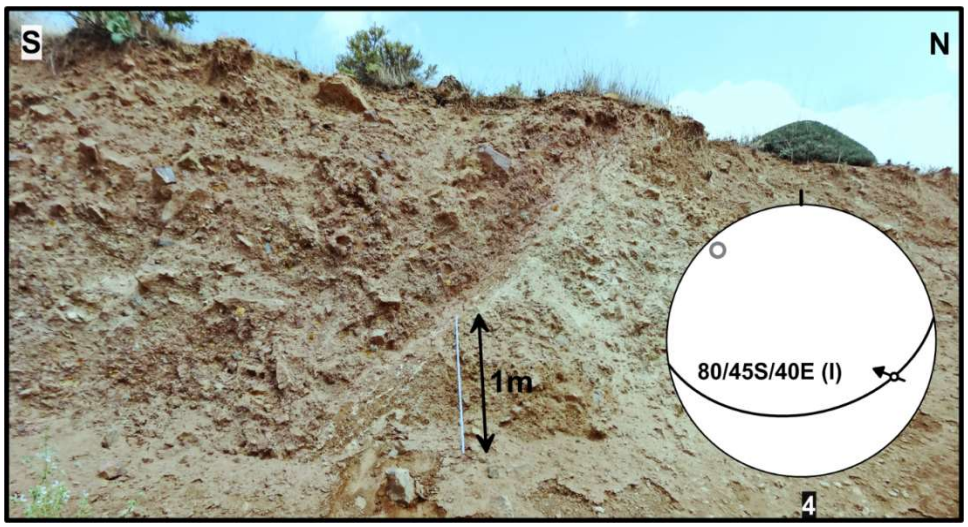

Figure 4. The measurements in Outcrop 4 defined compressive faulting with a dextral component that affected the glacial alluvium formations. The stereographic image of this fault at the right bottom shows an oblique reverse faulting with the right lateral component. The maximum stress of this faulting is oriented in the NW direction.

The SHmax orientation obtained from focal mechanisms data is primarily oriented 025 NE degrees on average. The stress regimes are estimated based on the relative position of the $\sigma 1$, $\sigma 2$, and $\sigma 3$ axes. The regional stress regime is, in general, strike-slip between 7 to 14 km depth and in this section, approaching the West, it changes to the reverse component and in the East, it becomes a pure strike-slip. At depth 0-7 km, the stress regime is transtensional; deeper than 14 km depth, it changes to transpressional (Figs. 6&7).

4. Discussion and conclusion

The field studies were examined at the hanging wall of the Mosha fault in the East of Mosha valley. Four outcrops of this fault were measured to evaluate precisely the faulting mechanism. The results obtained from this investigation can be summarized in the following points:

1. The outcrop of the Mosha fault displays two dips verging to the North and the South. Different faulting mechanisms obtained in this study and previous studies may be due to the S- and N-verging faults

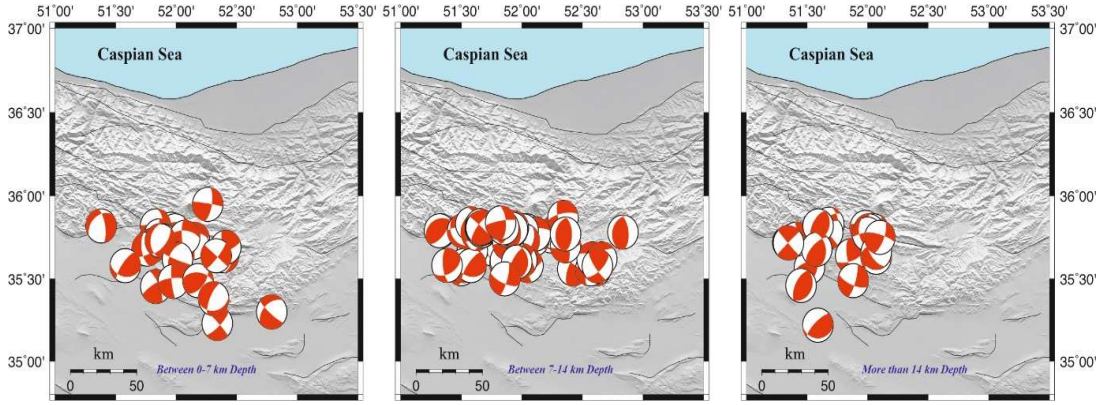

Figure 5. Distribution of the focal mechanisms used in the stress tensor inversion method in this study over the Central Alborz at 0-7 km, 7-14 km, and more than 14 km depth section from left to right.

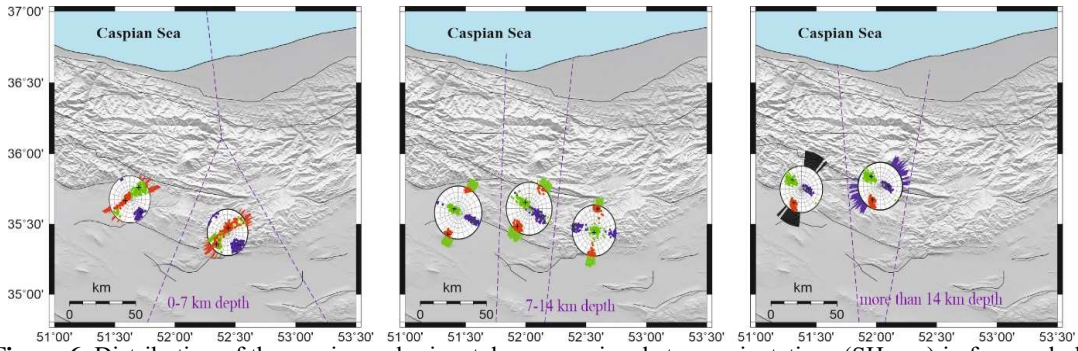

Figure 6. Distribution of the maximum horizontal compressional stress orientations (SHmax) in fan symbols and the principal stress orientations (Stereonets) in the selected region around the central Alborz at 0-7 km, 7-14 km and more than 14 km depth section from left to right. The variations in SHmax orientations show the uncertainty of a 95% confidence interval. The orientations are colour-coded in red, green, blue, and black, denoting normal, strike-slip, reverse, and oblique faulting, respectively. The maximum, intermediate, and minimum principal stresses in the stereonets are indicated with red, green, and blue, respectively. The purple dashed lines indicate the used Voronoi cells.

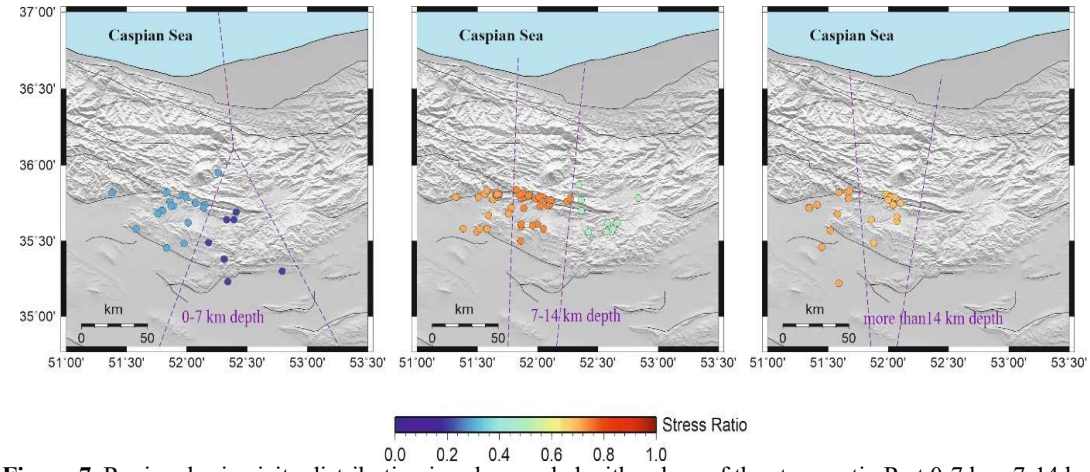

Figure 7. Regional seismicity distribution is colour coded with values of the stress ratio R at 0-7 km, 7-14 km, and more than 14 km depth section from left to right. In a strike-slip faulting environment, *R* values around 0.5, 0, and 1 indicate pure strike-slip, transtensional, and transpressional stress regimes, respectively. The purple dashed lines indicate the used Voronoi cells.

in a broad faulting zone.

2. Considering the young stress change in the Alborz, the determination of present-day stress should be undertaken by seismological study or measuring faults influencing the Late Pleistocene deposits.

3. Under the last stress direction (present-day stress), the faulting mechanism of the Mosha fault has changed to a normal left lateral mechanism (transtensional). On the other hand, the stress tensor obtained in this study employing focal mechanism inversion at 0-7 km depth demonstrates a transtensional stress regime. The recent study's results differ from Hessami's model (2020) in the Alborz. That model demonstrates that in the quaternary time, the basement faults are normal and in the cover, the faults remained reverse. However, this difference could be related to the implemented methods. Because the GPS data is related to the upper level, on the other hand, the depth uncertainty of the seismic data is in the kilometers dimension. Therefore, the stress situation may be different in the presence of seismic data at depths of less than one kilometer.

4. Before the establishment of the present-day stress, the Mosha fault was deformed under contractional deformation.

5. The change of vertical tectonic movements along the Mosha fault to a predominantly horizontal one is a relatively young tectonic re-arrangement (Late Pleistocene in age).

6. Regionally, the maximum horizontal stress (SHmax) orientation is directed at 025 NE on average. Stress ratio varies from transtensional stress regime in 0-7 km of the upper crust and changes in the lower crust toward transpressive.

7. The regional stress shows a strike-slip regime within 7-14 km depth beneath the Mosha fault, and it could be divided into two segments at the longitude of 52 (◦E). To the West, it changes to the reverse component, and in the East, it becomes a strike-slip.

8. The transpressional stress state observed at the basement, as well as the shallow transtensional faulting observed in the upper section suggest a shallow brittle crust.

Acknowledgments

The authors highly appreciate the Seismological Research Center at the International Institute of Earthquake Engineering and Seismology (IIEES) for supporting geological site visiting and providing waveform data for this research. Also, we acknowledge the Iranian Seismological

Center (IRSC) of the Institute of Geophysics at the University of Tehran for providing a part of the waveform data used in this paper. I would like to thank anonymous reviewers for constructive reviews, comments, and suggestions that led to numerous improvements in the final manuscript.

References

Abbassi, M.R., and Shabanian, E., 1999. Evolution of the stress field in the Tehran region during the Quaternary. In: Third International Conference on Seismology and Earthquake Engineering. Tehran, Iran.

Abbassi, M.R., 2020. Comparison of surface slip-data deduced from paleo-seismological sites and focal mechanisms in the South Central Alborz. Iranian Journal of Geophysics, **14(**2), 1-14. DOI:10.30499/IJG.2020.106199.

Allen, M.B., Vincent, S.J., Alsop, G.I., Ismail-zadeh, A. and Flecker, R., 2003. Late Cenozoic deformation in the South Caspian region: effects of a rigid basement block within a collision zone. Tectonophysics, **366**(3-4), 223-239.

Ambraseys, N.N. and Melville, C.P., 2005. A history of Persian earthquakes. Cambridge university press.

Bachmanov, D.M., Trifonov, V.G., Hessami, K.T., Kozhurin, A.I., Ivanova, T.P., Rogozhin, E.A., Hademi, M.C. and Jamali, F.H., 2004. Active faults in the Zagros and central Iran. Tectonophysics, **380**(3-4), pp.221-241.

Ballato, P., Uba, C.E., Landgraf, A., Strecker, M.R., Sudo, M., Stockli, D.F., Friedrich, A. and Tabatabaei, S.H., 2011. Arabia-Eurasia continental collision: Insights from late Tertiary foreland-basin evolution in the Alborz Mountains, northern Iran. Geological Society of America Bulletin, **123**(1-2), 106-131.

Berberian, M. and Yeats, R.S., 2001. Contribution of archaeological data to studies of earthquake history in the Iranian Plateau. Journal of Structural Geology, **23**(2-3), 563-584.

Bott, M. H. P., 1959. The mechanics of oblique-slip faulting. Geological Magazine, **96**(2), 109–117. https://doi.org/10.1017/S0016756800059987.

Hardebeck, J.L. and Michael, A.J., 2006. Damped regional-scale stress inversions: Methodology and examples for southern California and the Coalinga aftershock sequence. Journal of Geophysical Research: Solid Earth, **111**, B11310, doi:10.1029/2005JB004144.

Hessami, K., 2020. Polyphase Inversion Tectonics in Western Alborz Mountains, Northern Iran. Iranian Journal of Geophysics, **14**(4), 79-88.

Koyi, H., Nilfouroushan, F. and Hessami, K., 2016. Modelling role of basement block rotation and strike-slip faulting on the structural pattern in cover units of fold-and-thrust belts. Geological Magazine, **153**(5-6), 827-844.

Lund, B., & Townend, J., 2007. Calculating horizontal stress orientations with full or partial knowledge of the tectonic stress tensor. Geophysical Journal International, **170**(3), 1328–1335.

Martínez-Garzón, P., Ben-Zion, Y., Abolfathian, N., Kwiatek, G. and Bohnhoff, M., 2016. A refined methodology for stress inversions of earthquake focal mechanisms. Journal of Geophysical Research: Solid Earth, **121**(12), 8666-8687.

Martínez-Garzón, P., Kwiatek, G., Ickrath, M. and Bohnhoff, M., 2014. MSATSI: A MATLAB package for stress inversion combining solid classic methodology, a new simplified user-handling, and a visualization tool. Seismological Research Letters, **85**(4), 896-904.

Michael, A. J., 1984. Determination of stress from slip data: Faults and folds. Journal of Geophysical Research, **89**(B13), 11,517–11,526.

Michael, A.J., 1987. Use of focal mechanisms to determine stress: a control

study. Journal of Geophysical Research: Solid Earth, **92**(B1), 357-368.

Nemati, M., Hatzfeld, D., Gheitanchi, M.R., Sadidkhouy, A. and Mirzaei, N., 2011. Microseismicity and seismotectonics of the Firuzkuh and Astaneh faults (East Alborz, Iran). Tectonophysics, **506**(1-4), 11-21.

SoltaniMoghadam, S., Sepanloo, K. and Kheyri Moloumeh, M., 2018. Velocity model calculation and seismicity study of last decade on Tehran and high Alborz elevations. Iranian Journal of Geophysics, **12(**2), 78-95.

Tatar, M., Hatzfeld, D., Abbassi, A. and Fard, F.Y., 2012. Microseismicity and seismotectonics around the Mosha fault (Central Alborz, Iran). Tectonophysics, **544**, 50-59.

Tatar, M., Jackson, J., Hatzfeld, D. and Bergman, E., 2007. The 2004 May 28 Baladeh earthquake (M w 6.2) in the Alborz, Iran: overthrusting the South Caspian Basin margin, partitioning of oblique convergence, and the seismic hazard of Tehran. Geophysical Journal International, **170**(1), 249-261.

Tchalenko, J.S., Berberian, M., Iranmanesh, H., Bailly, M. and Arsovsky, M., 1974. Tectonic framework of the Tehran region. Geological Survey of Iran, Report #29.

Wallace, R. E., 1951. Geometry of shearing stress and relation to faulting. The Journal of Geology, **59**(2), 118 130. https://doi.org/10.1086/ 625831.

Yamini-Fard, F., Hosseini, M. and Norouzi, R., 2009. Seismicity of Tehran City Region and its Vicinity Based on Tehran City Seismic Network (TCSN) Data. Scientific Quarterly Journal of Geosciences, **19**(73), 133-138.

Zoback, M.L., 1992. First-and second-order patterns of stress in the lithosphere: The World Stress Map Project. Journal of Geophysical Research: Solid Earth, **97(**B8), 11703 -11728.